Improving heat transfer predictions in heterogeneous riparian zones using transfer learning techniques

Supplement

Aohan Jin[1], Wenguang Shi[1], Renjie Zhou[2], Hongbin Zhan[3], Quanrong Wang[1, 4*] and Xuan Gu[1]

[1]School of Environmental Studies, China University of Geosciences, Wuhan, Hubei, 430074, PR China.

[2]Department of Environmental and Geosciences, Sam Houston State University, Huntsville, TX 77340, USA.

[3]Department of Geology and Geophysics, Texas A&M University, College Station, TX 77843-3115, USA.

[4]MOE Key Laboratory of Groundwater Quality and Health, China University of Geosciences, Wuhan 430078, PR China.

Correspondence to: Quanrong Wang (wangqr@cug.edu.cn)

S1. Analytical solution of the 2D heat transfer process in homogeneous streambed

The mathematical model of Shi et al. (2023) accounts for thermal convection and thermal conduction in a homogeneous streambed, which can be described as follows:

$$\frac{\partial T}{\partial t} = D_x \frac{\partial^2 T}{\partial x^2} + D_z \frac{\partial^2 T}{\partial z^2} - v_x \frac{\partial T}{\partial x} - v_z \frac{\partial T}{\partial z}, x \geq 0, z \geq 0, t \geq 0 \quad \text{(S1)}$$

$$T(x, z, t = 0) = T(x, z) \quad \text{(S2)}$$

$$T(x, z = 0, t) = \begin{cases} f(t), 0 \leq x \leq L \\ 0, otherwise \end{cases} \quad \text{(S3)}$$

$$\left.\frac{\partial T}{\partial x}\right|_{x=0} = \left.\frac{\partial T}{\partial x}\right|_{x\to\infty} = \left.\frac{\partial T}{\partial z}\right|_{z\to\infty} = 0, t \geq 0 \quad \text{(S4)}$$

where T denotes temperature (℃); t is time (T); v_x and v_z refer to thermal front velocities (LT^{-1}) along the x- and z-axes, respectively. Specifically, $v_x = \frac{C_w}{C_s} q_x$, and $v_z = \frac{C_w}{C_s} q_z$, in which q_x and q_z denotes the components of water Darcy flux (LT^{-1}) components along the x- and z-axes, respectively; C_w and C_s are specific volumetric heat capacities (J/($m^3 \cdot$℃)) of water and streambed, respectively; D_x and D_z represent the effective thermal diffusivity along the x- and z- axes, respectively (L^2T^{-1}); L denotes the half width (L) of the river.

The above mathematical model can be analytically solved using the Green's function method. The solution of the temperature field can be written as:

$$T = A(x, z, t)\left[\int_0^\infty \int_o^L E(\lambda, \eta)\, B(x - \lambda, z - \eta, t) d\lambda d\eta + \int_o^t g(\tau) C(x, z, t - \tau) d\tau\right] \quad \text{(S5)}$$

$$A(x, z, t) = \frac{1}{4} exp\left[-\frac{v_z(v_z t - 2z)}{4D_z} - \frac{v_x(v_x t - 2x)}{4D_x}\right] \quad \text{(S6)}$$

$$B(x - \lambda, z - \eta, t) = \frac{1}{\pi t\sqrt{D_x D_z}}\left\{exp\left[-\frac{(z-\eta)^2}{4D_z t}\right] - exp\left[-\frac{(z-\eta)^2}{4D_z t}\right]\right\}$$
$$\left\{exp\left[-\frac{(x-\lambda)^2}{4D_x t}\right] + exp\left[-\frac{(x-\lambda)^2}{4D_x t}\right]\right\} \quad \text{(S7)}$$

$$C(x, z, t - \tau) = \frac{z}{\sqrt{\pi D_z (t-\tau)^3}} exp\left[-\frac{z^2}{4D_z(t-\tau)}\right]\left\{erf\left[\frac{L-x}{\sqrt{4D_x(t-\tau)}}\right] + erf\left[\frac{L+x}{\sqrt{4D_x(t-\tau)}}\right]\right\} \quad \text{(S8)}$$

$$E(\lambda, \eta) = h(\lambda, \eta) exp\left[-\frac{2\eta v_z}{4D_z} - \frac{2\lambda v_x}{4D_x}\right] \quad \text{(S9)}$$

$$g(\tau) = f(\tau)exp\left[\frac{v_z(v_z\tau)}{4D_z} + \frac{v_x(v_x\tau-2x)}{4D_x}\right] \quad \text{(S10)}$$

where λ, η, and τ represent dummy variables, which correspond to the independent variables x, z, and t, respectively. Detailed procedures of solution derivation can be found in Shi et al. (2023).

S2. Numerical solution of the 2D heat transfer process in heterogeneous streambed

A numerical model using COMSOL Multiphysics (COMSOL Inc., Burlington, MA, USA) is constructed to simulate heat transfer processes within homogeneous and heterogeneous streambeds. The domain of interest is discretized using triangular elements, with a finer spatial discretization near the river to reduce numerical truncation errors. The mesh consists of 16,998 triangular elements in total. A constant time step of 0.01 days is employed for the numerical solution. The following values are adopted from the study of Shi et al. (2023): $C_w = 4.18 \times 10^6 J/(m^3 \cdot °C)$, $C_s = 1.82 \times 10^6 J/(m^3 \cdot °C)$, $q_x = 0.2m/d$, $q_z = 0.3m/d$, $D_x = D_z = 7.69 \times 10^{-5} m^2/s$, $h(x,z) = 20°C$. To validate the developed numerical model, Figure S1 presents a comparison of temperature-time curves between the numerical and analytical solutions at three locations. Results indicate that the numerical solution closely aligns with the analytical solution, exhibiting small mean square error (MSE) values ranging from 0.06-0.11 ℃ for selected locations, thereby confirming the accuracy of the numerical solution. In the following analysis, the nonuniform flow and temperature fields are generated utilizing COMSOL Multiphysics, incorporating various heterogeneous lnK fields generated through an autocorrelated multi-Gaussian simulator.

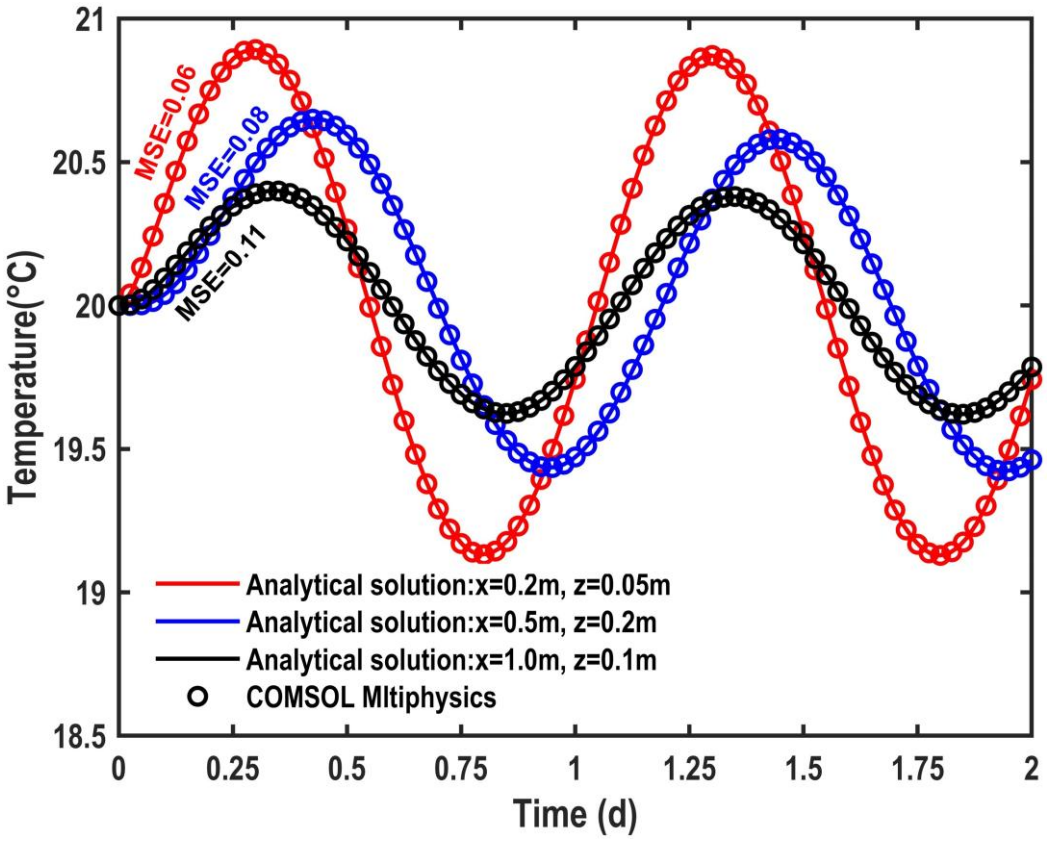

Figure S1. Comparison of temperature-time curves at three locations using the numerical solution (circle symbols) and the analytical solution of this study (solid curves).

S3. Prediction results with the DNN and PDTL models using 200 observation points

In this section, 200 observation points are used to evaluate the performance of the DNN and PDTL models. Figure S2 shows the prediction results with the DNN and the PDTL models using 200 observation points for homogeneous scenario. Figure S3 - S4 present the prediction results using 200 observation points for homogeneous scenario with the DNN and the PDTL models, respectively. Results demonstrate that there is no significant difference in the performance of the PDTL and DNN models for both homogeneous and heterogeneous scenarios when the number of observation points increases to 200. This suggests that with

enough data, DNNs can achieve similar results by learning data patterns that reduce the impact of physical information.

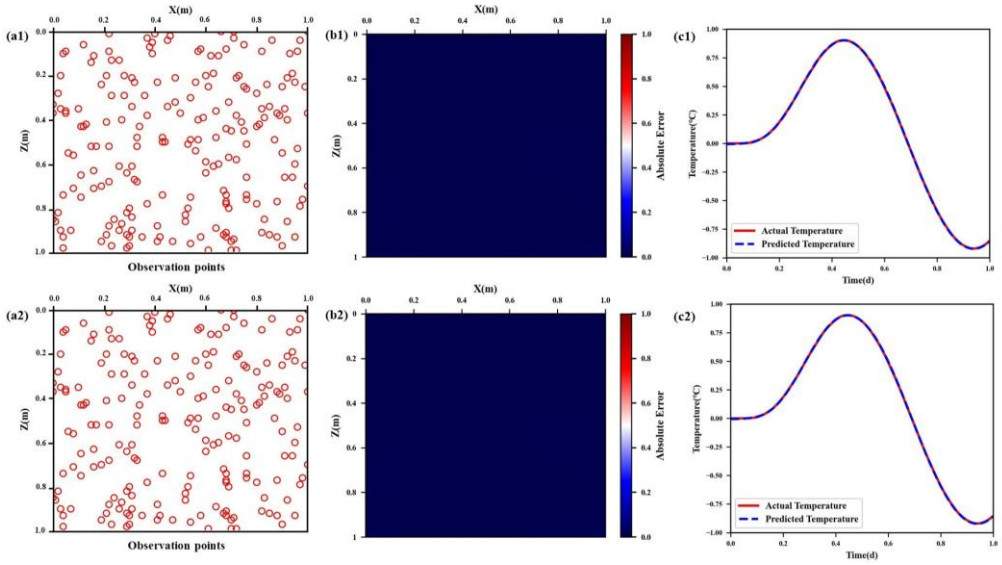

Figure S2. Prediction results with the DNN and the PDTL models using 200 observation points for homogeneous scenario. (a1) - (a2): the distribution of observation points with the DNN and the PDTL models; (b1) - (b2): the distribution of MAE predicted with the DNN and the PDTL models; (c1) - (c2): the temperature time series predicted with the PDTL and DNN models at $x = 0.5m,\ y = 0.5m$.

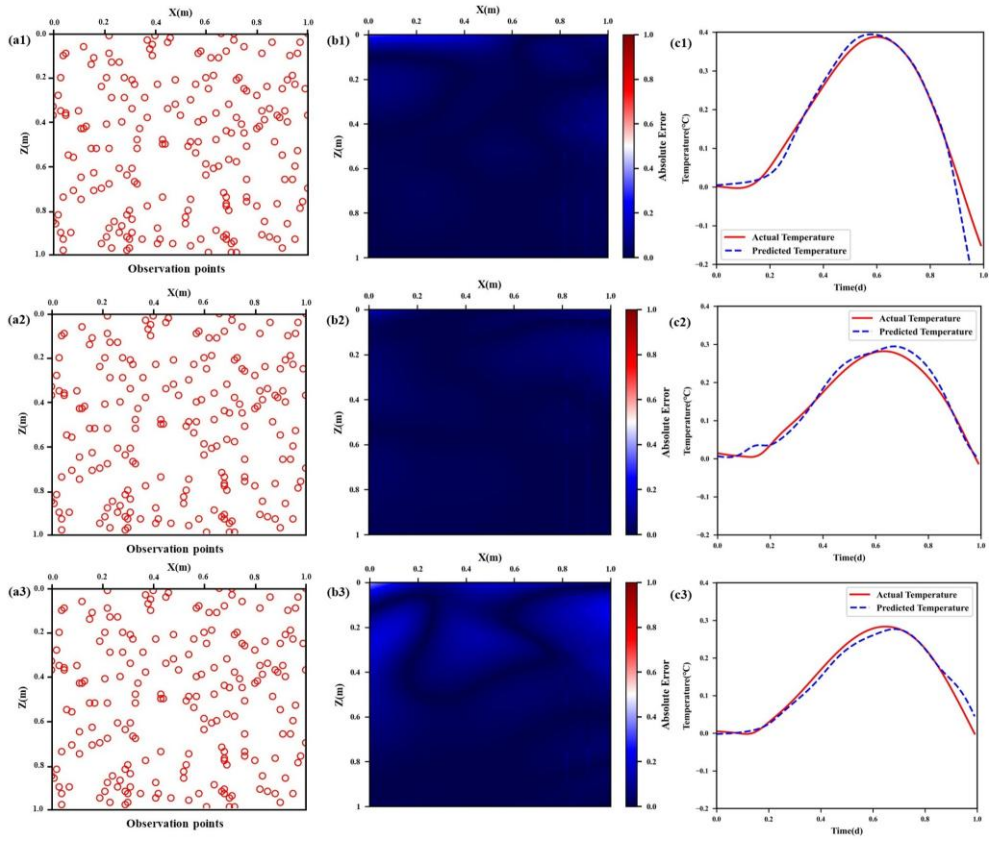

Figure S3. Prediction results with the DNN model using 200 observation points for heterogeneous scenarios. (a1) - (a3): the distribution of observation points with $\sigma_{lnk}^2 = 0.2$, 0.5, and 1.0; (b1) - (b3): the distribution of MAE predicted with $\sigma_{lnk}^2 = 0.2$, 0.5, and 1.0; (c1) - (c3): the temperature time series predicted with the PDTL and DNN models at $x = 0.5m$, $y = 0.5m$ with $\sigma_{lnk}^2 = 0.2$, 0.5, and 1.0.

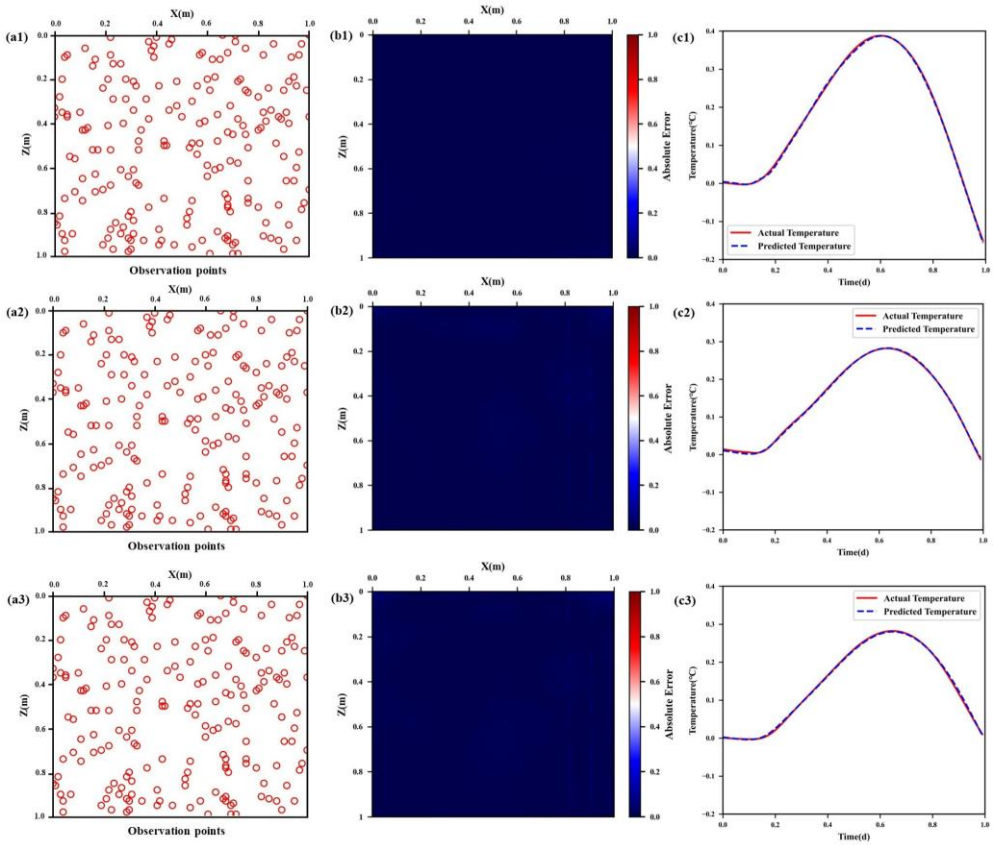

Figure S4. Prediction results with the PDTL model using 200 observation points for heterogeneous scenarios. (a1) - (a3): the distribution of observation points with $\sigma_{lnk}^2 = 0.2$, 0.5, and 1.0; (b1) - (b3): the distribution of MAE predicted with $\sigma_{lnk}^2 = 0.2$, 0.5, and 1.0; (c1) - (c3): the temperature time series predicted with the PDTL and DNN models at $x = 0.5m$, $y = 0.5m$ with $\sigma_{lnk}^2 = 0.2$, 0.5, and 1.0.

References

Shi, W., Zhan, H., Wang, Q., and Xie, X.: A two-dimensional closed-form analytical solution for heat transport with nonvertical flow in riparian zones, Water Resources Research, 59, e2022WR034059, https://doi.org/10.1029/2022WR034059, 2023.